Functional Lysine Modification by an Intrinsically Reactive Primary Glycolytic Metabolite

Raymond E. Moellering and Benjamin F. Cravatt

Science **341**, 549 (2013);
DOI: 10.1126/science.1238327

Science (print ISSN 0036-8075; online ISSN 1095-9203) is published weekly, except the last week in December, by the American Association for the Advancement of Science, 1200 New York Avenue NW, Washington, DC 20005.

Monkeys learned that one CS predicted only juice, whereas another predicted juice plus a simultaneous aversive stimulus (fig. S1C). Consistent with both hypotheses, the CS predicting juice alone caused a much stronger activation than the CS predicting juice plus saline or bitter (Fig. 3A). However, in contrast to the single-dimension hypothesis, prediction of air caused only a small suppression of the CS response in monkey F (Fig. 3B) and no suppression in monkey O (Fig. 3C). Across all 49 cells in monkey F in which experiments were performed both with air (Fig. 3B) and saline (Fig. 3A), the effect of saline (in suppressing firing rates) was significantly greater than that of air ($P = 0.02$, paired t test). When air was delivered together with juice but with a probability of 0.5 (following a CS), its aversiveness had no effect on firing rate (Fig. 3D). Analogous experiments in which a loud (90 dB) but neutral sound replaced air yielded similar results, with the sound being ineffectual (fig. S3).

The insensitivity of dopamine neurons to aversiveness suggests that other neurons should represent aversiveness. Reward and aversiveness could be represented independently by discrete sets of neurons because they are experienced by the brain as statistically independent of one another, displaying neither strong positive nor negative correlations. They would not be represented as opposites along a single dimension because in general, they are not anticorrelated with one another. This is essentially the same explanation that has been given for receptive field formation in sensory systems, in which distinct neurons learn to recognize statistically independent features as discrete "objects" (*26*, *27*).

Past and present results do support the existence of opponent representations for reward (*3*, *13*, *16*, *28*), and the same is likely to be the case for aversiveness. Thus, one can infer from the present results that there are four types of value representations, which could be denoted as reward-ON (R_{ON}), reward-OFF (R_{OFF}), aversive-ON (A_{ON}), and aversive-OFF (A_{OFF}). The "ON" neurons would be activated by evidence for reward, or for aversiveness, and the "OFF" neurons by evidence against reward, or against aversiveness. These four putative types of neurons would mediate the four types of reinforcement distinguished at the behavioral level. Skinner denoted these, esoterically, as positive reinforcement (R_{ON}), positive punishment (A_{ON}), negative reinforcement (A_{OFF}), and negative punishment (R_{OFF}) (*1*). Because dopamine represents R_{ON}, it is natural to ask whether the other three major modulatory neurotransmitters might represent the other three value signals. Although some recordings have been made from neurons containing norepinephrine, serotonin, and acetylcholine, it remains uncertain how they represent value, in part because of the challenges described above in characterizing neuronal responses to both reward and aversiveness. Regardless of the other classic neuromodulators, the present results suggest the existence of at least three other modulatory signals to represent the other three aspects of value and to "teach" value throughout large parts of the brain in a manner analogous to that proposed for dopamine (*2*, *7*, *9*).

References and Notes

1. B. F. Skinner, *Contingencies of Reinforcement: A Theoretical Analysis* (Appleton-Century-Crofts, New York, 1969).
2. W. Schultz, P. Dayan, P. R. Montague, *Science* **275**, 1593–1599 (1997).
3. N. D. Daw, S. Kakade, P. Dayan, *Neural Netw.* **15**, 603–616 (2002).
4. M. Joshua, A. Adler, R. Mitelman, E. Vaadia, H. Bergman, *J. Neurosci.* **28**, 11673–11684 (2008).
5. M. Moutoussis, R. P. Bentall, J. Williams, P. Dayan, *Network* **19**, 137–160 (2008).
6. M. Matsumoto, O. Hikosaka, *Nature* **459**, 837–841 (2009).
7. P. Dayan, Q. J. M. Huys, *Annu. Rev. Neurosci.* **32**, 95–126 (2009).
8. E. S. Bromberg-Martin, M. Matsumoto, O. Hikosaka, *Neuron* **68**, 815–834 (2010).
9. P. W. Glimcher, *Proc. Natl. Acad. Sci. U.S.A.* **108** (suppl. 3), 15647–15654 (2011).
10. E. B. Oleson, R. N. Gentry, V. C. Chioma, J. F. Cheer, *J. Neurosci.* **32**, 14804–14808 (2012).
11. S. Ravel, E. Legallet, P. Apicella, *J. Neurosci.* **23**, 8489–8497 (2003).
12. J. J. Paton, M. A. Belova, S. E. Morrison, C. D. Salzman, *Nature* **439**, 865–870 (2006).
13. M. Matsumoto, O. Hikosaka, *Nat. Neurosci.* **12**, 77–84 (2009).
14. S. E. Morrison, C. D. Salzman, *J. Neurosci.* **29**, 11471–11483 (2009).
15. T. C. Jhou, H. L. Fields, M. G. Baxter, C. B. Saper, P. C. Holland, *Neuron* **61**, 786–800 (2009).
16. C. D. Fiorillo, M. R. Song, S. R. Yun, *J. Neurosci.* **33**, 4710–4725 (2013).
17. C. D. Fiorillo, S. R. Yun, M. R. Song, *J. Neurosci.* **33**, 4693–4709 (2013).
18. P. N. Tobler, C. D. Fiorillo, W. Schultz, *Science* **307**, 1642–1645 (2005).
19. J. Mirenowicz, W. Schultz, *Nature* **379**, 449–451 (1996).
20. D. V. Wang, J. Z. Tsien, *PLoS ONE* **6**, e17047 (2011).
21. J. Y. Cohen, S. Haesler, L. Vong, B. B. Lowell, N. Uchida, *Nature* **482**, 85–88 (2012).
22. Materials and methods are available as supplementary materials on *Science* Online.
23. Of 195 dopamine neurons, 134 were from monkey O, and 61 were from monkey F. It was estimated that 81, 13, and 6% were in substantia nigra, ventral tegmental area, and retrorubral field, respectively, with 45% of all neurons being in the "ventral tier" (ventral substantia nigra compacta and reticulata) and the other 55% being in the "dorsal tier" (*17*).
24. C. D. Fiorillo, *Neuroscience* **197**, 162–171 (2011).
25. P. N. Tobler, A. Dickinson, W. Schultz, *J. Neurosci.* **23**, 10402–10410 (2003).
26. B. A. Olshausen, D. J. Field, *Nature* **381**, 607–609 (1996).
27. A. J. Bell, T. J. Sejnowski, *Vision Res.* **37**, 3327–3338 (1997).
28. S. Hong, T. C. Jhou, M. Smith, K. S. Saleem, O. Hikosaka, *J. Neurosci.* **31**, 11457–11471 (2011).

Acknowledgments: I thank W. T. Newsome for advice and helpful discussions, J. R. Brown for excellent technical assistance, and W. A. Phillips, J. R. Wickens, and M. R. Song for constructive comments on the manuscript. Research was supported by grants from the Basic Science Research Program (2012R1A1A2006996) and World Class University (WCU) program (R32-2008-000-10218-0) of the National Research Foundation of Korea (NRF) funded by the Ministry of Education, Science and Technology, and a grant to W. T. Newsome from the Howard Hughes Medical Institute.

Supplementary Materials

www.sciencemag.org/cgi/content/full/341/6145/546/DC1
Materials and Methods
Figs. S1 to S3
Reference (*29*)

3 April 2013; accepted 4 June 2013
10.1126/science.1238699

Functional Lysine Modification by an Intrinsically Reactive Primary Glycolytic Metabolite

Raymond E. Moellering and Benjamin F. Cravatt

The posttranslational modification of proteins and their regulation by metabolites represent conserved mechanisms in biology. At the confluence of these two processes, we report that the primary glycolytic intermediate 1,3-bisphosphoglycerate (1,3-BPG) reacts with select lysine residues in proteins to form 3-phosphoglyceryl-lysine (pgK). This reaction, which does not require enzyme catalysis, but rather exploits the electrophilicity of 1,3-BPG, was found by proteomic profiling to be enriched on diverse classes of proteins and prominently in or around the active sites of glycolytic enzymes. pgK modifications inhibit glycolytic enzymes and, in cells exposed to high glucose, accumulate on these enzymes to create a potential feedback mechanism that contributes to the buildup and redirection of glycolytic intermediates to alternate biosynthetic pathways.

Regulation of protein structure and function by reversible small-molecule binding (*1*, *2*) and covalent posttranslational modification (PTM) (*3*) are core tenets in biochemistry. Many intermediates in primary metabolic pathways reversibly bind to proteins as a form of feedback or feedforward regulation (*2*). Covalent PTMs are, however, typically introduced onto proteins by enzyme-catalyzed processes, but can also result from enzyme-independent interactions between reactive metabolites and nucleophilic residues in proteins (*4*–*7*). The scope and broad functional significance of nonenzymatic modifications of proteins, however, remain poorly understood. In this context, we wondered whether intrinsically reactive intermediates in primary

metabolic pathways might covalently modify proteins.

A survey of primary metabolites with the potential to modify proteins focused our attention on the central glycolytic intermediate 1,3-bisphosphoglycerate (1,3-BPG), a product of catalysis by glyceraldehyde-3-phosphate dehydrogenase (GAPDH) that has a highly electrophilic acylphosphate group (Fig. 1A). Acylphosphate reactivity is central to several enzyme-catalyzed metabolic processes (*8*, *9*) and has proven useful in the design of electrophilic nucleotide probes that react with conserved lysines within kinase active sites (*10*). We thus examined whether 1,3-BPG might modify lysine residues on proteins to form 3-phosphoglyceryl-lysine (pgK) (Fig. 1A).

Because of its propensity for rearrangement to the more stable isomer 2,3-bisphosphoglycerate (2,3-BPG), 1,3-BPG is not commercially available. Therefore, to initially determine whether 1,3-BPG reacted with proteins to form pgK modifications, we produced this metabolite in situ by incubating purified human GAPDH with substrate and cofactor (fig. S1). GAPDH was then trypsinized and analyzed by liquid chromatography–tandem mass spectrometry (LC-MS/MS) on an Orbitrap Velos mass spectrometer for peptides with a differential modification mass of 167.98238 daltons on lysines, the expected mass shift caused by pgK formation. Several pgK-modified GAPDH peptides were identified in reactions with substrate and cofactor (GGN conditions) (Fig. 1B and table S1). These pgK-modified peptides were much less abundant, but still detectable in control reactions lacking substrate (GN) or cofactor (GG), which suggested that commercial GAPDH, which is purified from erythrocytes, may be constitutively pgK-modified. Structural assignments for two distinct pgK-modified GAPDH peptides were verified by comparison with synthetic peptide standards (fig. S2, see Materials and Methods), which showed equivalent LC retention times and MS/MS spectra (Fig. 1C and figs. S3 and S4). Analysis of a GAPDH crystal structure revealed that all of the pgK-modified lysines are solvent-exposed (fig. S5) and that the most frequently identified sites of modification (K107, K194, and K215) (table S1) cluster around the GAPDH active site (Fig. 1D). Isoelectric focusing (IEF) revealed a shift in the isoelectric point (pI) distribution of GAPDH from ~8.6 in GN control reactions to 6.5 to 7.66 in GGN reactions (Fig. 1E and fig. S6). This shift is consistent with GAPDH's having acquired a net negative change in charge through capping of lysines by phosphoglycerate, a conclusion also supported by LC-MS/MS analysis, which revealed substantial enrichment of pgK-modified peptides in the acidic IEF fractions (fig. S6).

We next assessed the existence and global distribution of pgK modifications in cell proteomes. We reasoned that pgK-peptides might share enough physicochemical properties with phosphorylated peptides to permit enrichment by a standard phosphoproteomic workflow that used immobilized metal affinity chromatography (IMAC) (fig. S7) (*11*). pgK-modified lysines were identified in several protein classes in four human cell lines examined (table S2). Two of the aforementioned pgK-sites observed for GAPDH in vitro were detected in human cells and generated MS/MS spectra that matched the spectra of both the synthetic (fig. S8) and in vitro–derived (figs. S3 and S4) pgK-modified GAPDH peptides. Meta-analysis of published phosphoproteomic data sets (*12*, *13*) confirmed that pgK-modified proteins are also present in normal mouse tissues and that several pgK sites are conserved in human and mouse protein orthologs (Fig. 2, A and B, and table S3). Bioinformatic clustering with DAVID software (*14*) and KEGG pathway analysis revealed enrichment of pgK-modified proteins in glycolysis in both human cells (Fig. 2C and table S4) and mouse liver (Fig. 2D and table S4).

Examination of the observed modification sites revealed that they often occurred on catalytic or regulatory lysine residues in the active sites of glycolytic enzymes that use three-carbon substrates (Fig. 2, A, B, and E; and fig. S9). Notable exceptions were phosphoglycerate kinase (PGK1) and bisphosphoglycerate mutase (BPGM), both of which accept 1,3-BPG as a substrate but have active sites predominantly made up of histidine and arginine residues (fig. S10). These findings suggest that both PGK1 and BPGM may have evolved to have active sites that are resistant to stable modification by 1,3-BPG. Analysis of the local sequence context surrounding

The Skaggs Institute for Chemical Biology and Department of Chemical Physiology, The Scripps Research Institute, La Jolla, CA 92037, USA.

*Corresponding author. E-mail: cravatt@scripps.edu (B.F.C.); rmoeller@scripps.edu (R.E.M.)

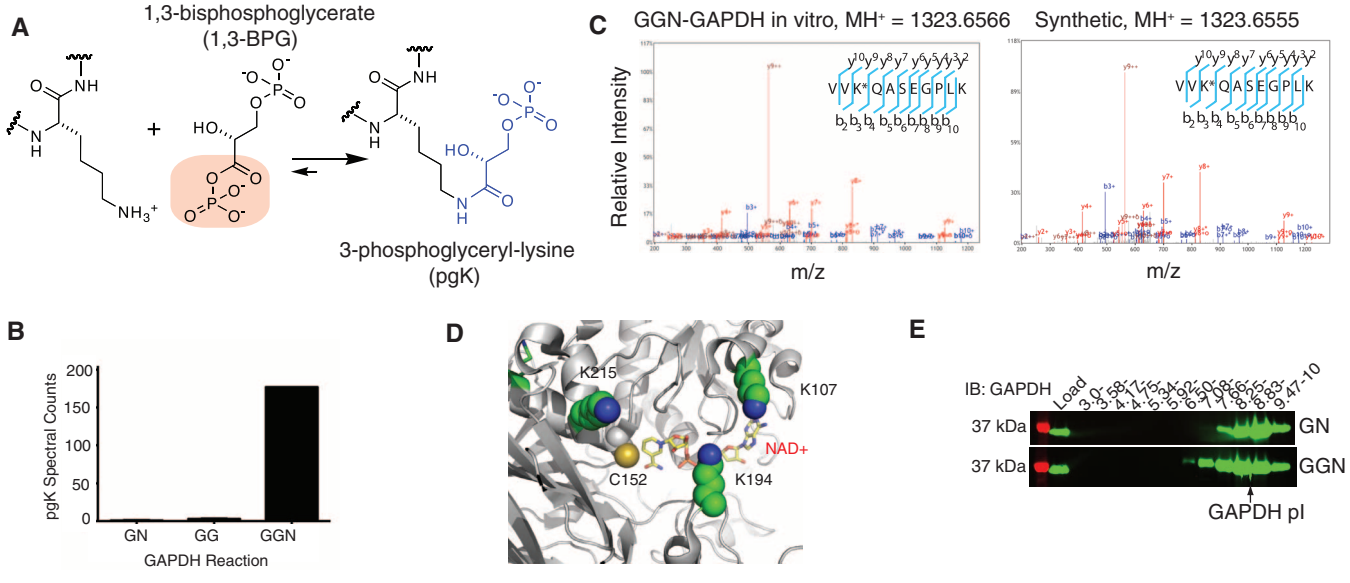

Fig. 1. 1,3-BPG forms a stable, covalent modification on lysines of GAPDH in vitro. (**A**) pgK formed by reaction of a lysine ε-amine with the acylphosphate functionality in 1,3-BPG. (**B**) Spectral counts of pgK-modified tryptic peptides detected by LC-MS/MS analyses of GN, GG, and GGN GAPDH enzymatic reactions (average of two independent experiments). (**C**) MS/MS spectra of the in vitro GGN-GAPDH–derived (left) and synthetic (right) doubly charged tryptic peptide VV(pg)KQASEGPLK. Observed b-, y-, and relevant parent ions, as well as products of dehydration (°) or ammonia loss (*) are labeled. Asterisk (*) within peptide sequences denotes the pgK-modified lysine. (**D**) The most frequently detected pgK-modification sites (K107, K194, and K215) surround the active site of GAPDH [Protein Data Bank (PDB) accession no. 1ZNQ]. (**E**) Western immunoblot (IB) with antibody against GAPDH in GG- and GGN-GAPDH reactions after IEF analysis. Data are from a representative experiment of three independent experiments.

pgK sites revealed no discernible motif (fig. S11), which is consistent with an enzyme-independent labeling mechanism.

Metabolic labeling with heavy glucose (D-glucose-$^{13}C_6$, 1, 2, 3, 4, 5, 6, 6-d_7) revealed that pgK modifications were derived from glucose metabolism (fig. S12). We next tested whether changes in glycolytic flux, through altering 1,3-BPG, might dynamically regulate the extent of pgK modifications in cells. We exposed cells to normal (10 mM) or high (25 mM) concentrations of glucose and found that the latter cells, which had 4- to 5-fold elevations in bis-(1,3 and/or 2,3-)phosphoglycerate (Fig. 3A), exhibited greater pgK signals for several proteins (Fig. 3B), as judged by immunoblotting with antibodies generated against pgK (fig. S13 and Materials and Methods). Similar experiments performed on human embryonic kidney–293T (HEK293T) cells expressing FLAG-tagged ENO1 or GAPDH revealed that both proteins showed significant glucose concentration–dependent increases in their pgK-modification state (Fig. 3, C and D). We also used the quantitative proteomic method SILAC [stable isotope labeling of amino acids in cell culture (*15*)] and found that cells grown in 25 mM glucose exhibited increased pgK modification of several proteins, including the active-site lysine of ENO1, K343, without changes in the abundance of non-pgK peptides in these proteins (Fig. 3, E and F; table S5; and fig. S14). IEF further established a shift in ENO1 protein to more acidic pH fractions in cells grown in 25 mM glucose (Fig. 3G). Finally, analysis of mouse phosphoproteomic data sets (*12*) revealed that the extent and distribution of pgK modifications for glycolytic enzymes, as measured by pgK-peptide spectral counts, were highest in liver, brain, and kidney, which are major sites of glucose uptake and glycolytic and gluconeogenic activity in vivo (Fig. 3H, fig. S15, and table S3) (*16*).

We detected pgK modification of multiple nuclear proteins (tables S2 and S3 and figs. S14C and S16A). GAPDH can localize to the nucleus (*17*), and this distribution is promoted by exposing cells to high concentrations of glucose (*18*, *19*) (fig. S16, B and C), which provides a potential mechanistic explanation for the glucose-stimulated increase in pgK signals for the nuclear protein NUCKS1 (nuclear ubiquitous casein and cyclin-dependent kinases substrate 1) (figs. S14C and S16D). We further tested this premise by comparing nuclear pgK profiles in HEK293T cells transfected with wild-type (GAPDH-WT) or nuclear-localized GAPDH (GAPDH-NLS, containing a C-terminal SV40 nuclear localization sequence) (fig. S16, E to G). GAPDH-NLS cells exhibited increased pgK signals in a subset of nuclear proteins (fig. S16H), including NUCKS1 (fig. S16I).

We next assessed the impact of pgK modification on glycolytic enzyme activity. We first compared in vitro pgK-modified (GGN) with control (GN) GAPDH reactions after dialysis to remove unreacted 1,3-BPG and other metabolites. GAPDH from GGN reactions exhibited an approximately twofold increase in apparent Michaelis constant (K_m) value (Fig. 4A), indicating that pgK modifications may perturb interactions with GAP substrate. We attempted to mimic 1,3-BPG modification of the catalytic lysine (K343) of ENO1 (*20*), as well as another active site lysine (K394) (Fig. 4B), by generating K-to-E mutations, which displayed substantially reduced activity (Fig. 4C and fig. S17A). We also found that FLAG-tagged ENO1 enzyme expressed in HEK293T cells showed ~30% lower activity after exposure to 25 mM versus 10 mM glucose for 24 hours (Fig. 4D), which is consistent with our quantitative proteomic findings indicating enhanced pgK modification of K343 in cells exposed to high glucose concentrations (Fig. 3C, E-G).

We used targeted metabolomics (table S6) to measure glycolytic and citric acid cycle (CAC) intermediates in human cells exposed to 10 versus 25 mM glucose for 24 hours and, as expected, found higher concentrations of metabolites in the latter condition. However, these increases were not uniform but were mostly restricted to central

A Human Cell Lines

Protein	Residue	Sequence	Annotation
glycolysis			
GAPDH	K263	K.VV(pg)KQASEGPLK.G	ubiquitylation site
GAPDH	K215	R.GALQNIIPASTGAA(pg)KAVGK.V	active site
ENO1	K343	K.SCNCLLL(pg)KVNQIGSVTESLQACK.L	catalytic lysine
PGAM1	K100	R.HYGGLTGLN(pg)KAETAAK.H	active site
PKM2	K367	R.AEGSDVANAVLDGADCIMLSGETA(pg)KGDYPLEAVR.M	active site
protein translation			
RPLP2	K99	K.(pg)KEESEESDDDMGFGLFD.-	-

B Mouse Liver

Protein	Residue	Sequence	Annotation
glycolysis			
Gapdh	K261	K.VV(pg)KQASEGPLK.G	ubiquitylation site
Gapdh	K213	R.GAAQNIIPASTGAA(pg)KAVGK.V	active site
Aldob	K147	K.DGVDFG(pg)KWR.A	active site
Pgam1	K100	R.HYGGLTGLN(pg)KAETAAK.H	active site
Eno1	K343	K.SCNCLLL(pg)KVNQIGSVTESLQACK.L	catalytic lysine
protein translation			
Rplp1	K98	K.(pg)KEESEESEDDMGFGLFD.-	-

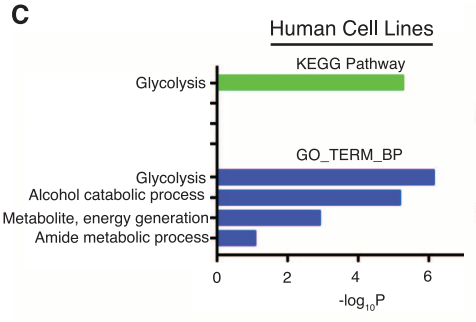

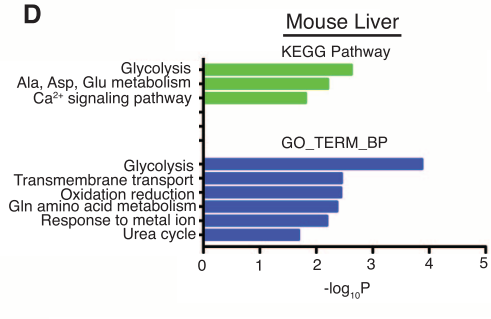

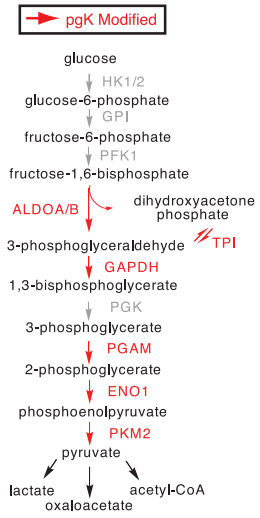

Fig. 2. Functional distribution of pgK-modification sites in human cells and mouse tissues. (**A** and **B**) Modification site, peptide sequence, and associated annotation for representative endogenous pgK-modified proteins from human cell lines (A) and mouse liver (B). "(pg)K" denotes the pg-modified lysine. (**C** and **D**) Gene ontology biological process categories (GOTERM_BP) and KEGG pathways enriched among pgK-modified proteins in human cell lines (C) and mouse liver (D) by DAVID bioinformatic analysis. (**E**) Schematic of observed pgK-modified enzymes in glycolysis. Glycolytic enzymes containing at least one pgK site are shown in red, others are shown in gray.

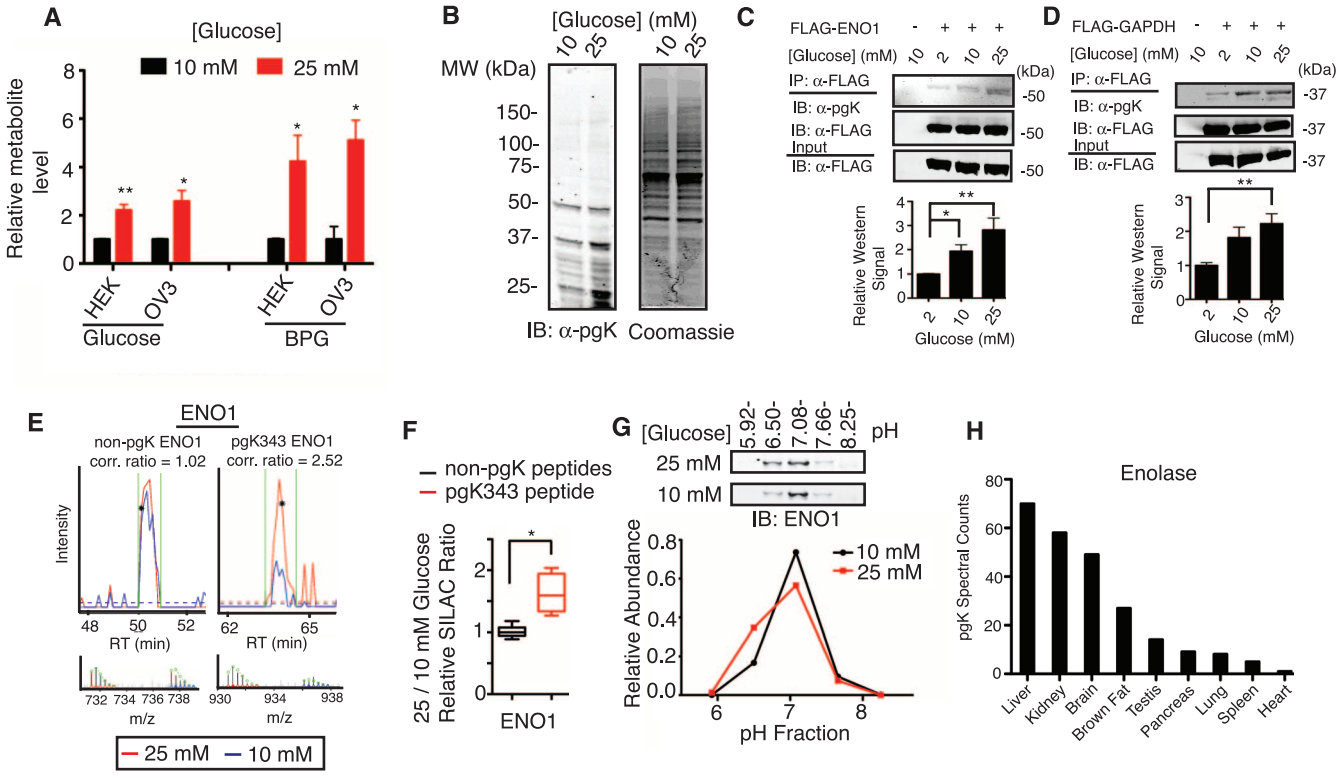

Fig. 3. Dynamic coupling of pgK modification to glucose metabolism. (**A**) Intracellular glucose and bisphosphoglycerate (BPG, aggregate of both 1,3- and 2,3-isomers) levels from cells grown at indicated glucose concentrations for 24 hours. (**B**) Antibody against pgK (α-pgK) IB and Coomassie-stained gel of proteomes from HEK293T cells grown at indicated glucose concentrations. (**C** and **D**) α-pgK IB of α-FLAG–enriched ENO1 (C) and GAPDH (D) expressed in HEK293T cells grown at indicated glucose concentrations. Shown below each blot is a graph of the average relative α-pgK band intensities (n = 4 per group). (**E**) Representative SILAC chromatograms, MS1 isotope envelopes, and corrected (corr.) area ratios for non-pgK (left) and pgK-modified (right) peptides from ENO1. Integration area is shown within green bars; asterisk (*) in the chromatogram signifies the triggered MS2 scan. (**F**) Average SILAC ratios for pgK343-containing and non-pgK ENO1 peptides from cells grown at indicated glucose concentrations. Horizontal line and whiskers represent the mean and 10 to 90% confidence intervals, respectively. (**G**) IB of IEF-focused ENO1 from MCF7 cells grown at the indicated glucose concentrations. Plot shows the IEF-focused ENO1 pI distributions quantified by densitometry. (**H**) Spectral count values for pgK-modified enolase peptides across nine mouse tissues (table S3). Data represent means ± SEM; statistical significance was determined by two-way t tests with a Bonferroni correction for (C) and (D) and Welch's correction for (F): *P < 0.05; **P < 0.01; ***P < 0.005.

glycolytic metabolites, including fructose-1,6-bisphosphate (FBP), glyceraldehyde-3-phosphate (GAP), phosphoglycerate (both 2- and 3-isomers, 2PG and 3PG) and phosphoenolpyruvate (PEP) (Fig. 4E and fig. S17, B to D). A similar metabolomic profile was observed in cells cultured in normal glucose and treated with the ENO1 and PKM2 inhibitor NaF (3 mM, 24 hours) (fig. S17, E to G). We used pulse-chase experiments with 10 mM ^{13}C-labeled glucose to measure glycolytic flux in cells grown in 10 versus 25 mM glucose for 24 hours. Cells grown in 25 mM glucose showed reduced glycolytic flux at early time points postchase with ^{13}C-glucose (≤ 6 hours) and these decreases were alleviated by 16 hours (Fig. 4F), which correlated with changes in pgK-signals over the time course (fig. S17H, I). Finally, the build up of glycolytic metabolites in cells exposed to either high glucose or NaF was accompanied by increased concentrations of metabolites that are biosynthesized from central glycolytic intermediates, including serine, ribulose-5-phosphate, and reduced glutathione (Fig. 4G and fig. S17J).

We found that a synthetic, pgK-containing tetrapeptide Ac-AA(pg)KA (fig. S18A) was deacylated (Ac-AAKA) and dephosphorylated [Ac-AA(g)KA; glyceryl-lysine, (g)K] when exposed to native, but not heat-denatured, cell lysates or buffer alone (fig. S18, B and C), which indicated that pgK modifications can be enzymatically metabolized. Broad-spectrum phosphatase inhibitors blocked formation of dephosphorylated and, to a lesser extent, deacylated peptide products (fig. S18D), which suggested that deacylation may occur directly from pgK-peptides or through a dephosphorylated gK intermediate (fig. S18E). Kinetic analysis in cell lysates further revealed that deacylation and dephosphorylation reactions occur on similar time scales in cell lysates (fig. S18F). These data indicate that pgK is a dynamic and reversible PTM.

In summary, we have identified herein a PTM found on numerous mammalian proteins (tables S2 and S3) that originates from the reaction of lysines with a primary glycolytic metabolite, 1,3-BPG. This reaction increases the size and inverts the charge potential of the modified residue from positive to negative and, therefore, has the potential to affect the structure and function of proteins from diverse families and pathways (fig. S19). 1,3-BPG modification of lysines also likely occurs in lower organisms, given the conservation of glycolysis throughout evolution (*21*, *22*). The enrichment of pgK-modification sites on glycolytic enzymes indicates that these enzymes may form a physical complex in cells (*23*), as has been observed for other metabolic pathways (*24*). The localization of GAPDH to additional subcellular structures or protein complexes could provide a general mechanism to regulate the pgK-modification state of proteins. An aggregate effect of partial enzyme impairments by pgK modification in the glycolytic pathway may be reduced carbon flow into Lac and CAC intermediates, which leads to increased levels of central metabolites that can be shunted to alternate biosynthetic pathways (fig. S20) (*25*, *26*). Erythrocytes isolated from patients with a rare deficiency in BPGM, which should increase 1,3-BPG concentrations, show a profile similar to that of cells grown in high concentrations of glucose, with build-up of

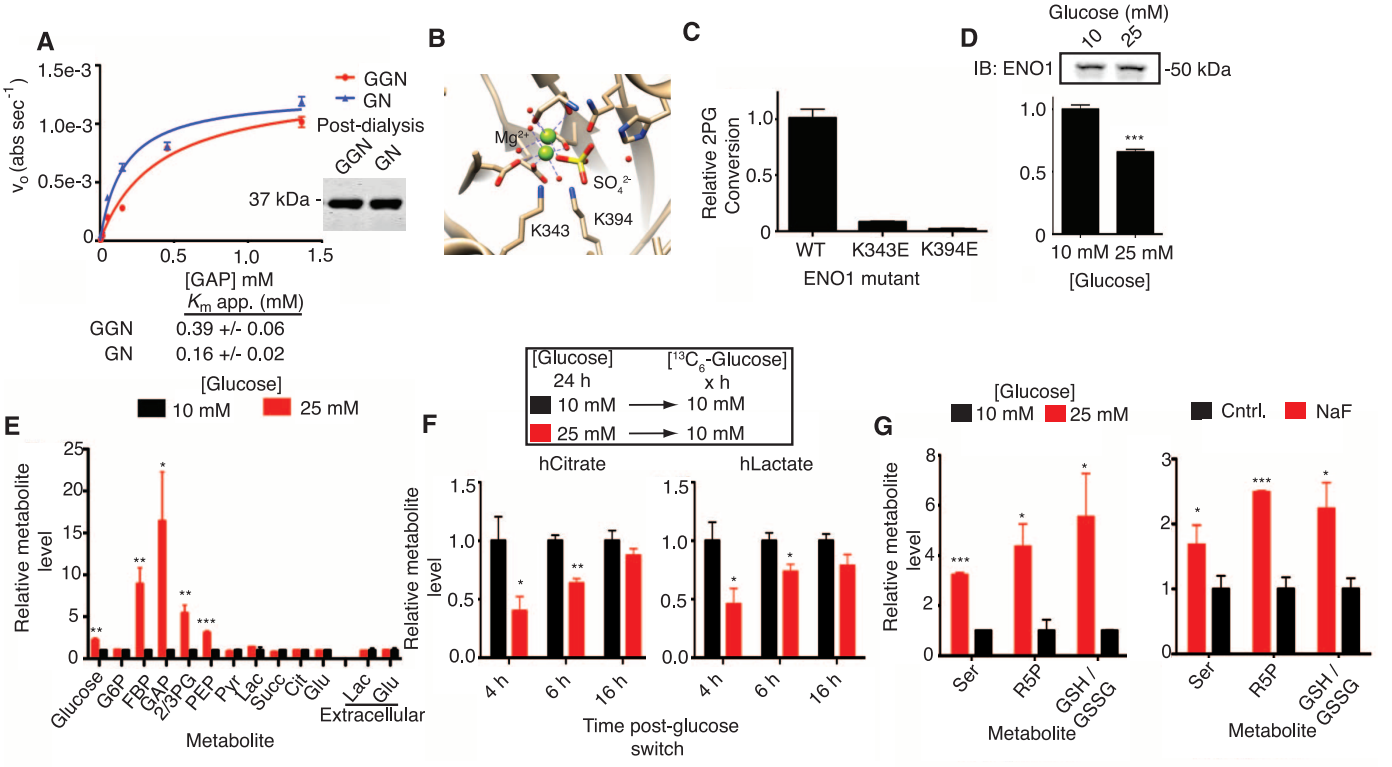

Fig. 4. pgK modification impairs glycolytic enzymes and correlates with altered glycolytic output in human cells. (**A**) Michaelis-Menten kinetic analysis comparing GAPDH from GGN (1,3-BPG–producing) with GN (control) reactions. v_0, initial enzyme velocity measurements. (**B**) Structure of ENO1 active site (PDB accession no. 3B97) showing residues important for catalysis, including pgK sites K343 and K394. (**C**) Relative activities of wild-type and mutant FLAG-tagged ENO1 expressed and affinity-isolated from HEK293T cells (fig. S17A for expression data of ENO1 variants). (**D**) Relative activities of FLAG-isolated ENO1 expressed in HEK293T cells cultured in 10 versus 25 mM glucose for 24 hours. (**E**) Relative metabolite levels in HEK293T cells grown in 10 versus 25 mM glucose for 24 hours. (**F**) Relative heavy lactate and citrate levels in HEK293T cells pretreated with the indicated glucose concentrations for 24 hours and then grown in 10 mM heavy glucose for the indicated length of time. (**G**) Relative metabolite measurements in cells grown in 10 versus 25 mM glucose (left) or treated with NaF (right). Data shown represent means ± SEM from triplicate experiments. Statistical significance was determined by two-way *t* tests: $*P < 0.05$; $**P < 0.01$; $***P < 0.005$; n.s., not significant. G6P, glucose-6-phosphate; FBP, fructose-1,6-bisphosphate; Pyr, pyruvate; Lac, lactate; Succ, succinate; Cit, citrate; Glu, glutamate; Ser, serine; R5P, ribulose-5-phosphate; GSH/GSSG, reduced/oxidized glutathione.

the central metabolites FBP, glyceraldehyde-3-phosphate (GAP), 2PG, 3PG, and PEP (*27*). Thus, pgK modifications could constitute an intrinsic feedback mechanism by which a reactive central metabolite (1,3-BPG) regulates product distribution across the glycolytic pathway in response to changes in glucose uptake and metabolism.

References and Notes

1. L. Swint-Kruse, K. S. Matthews, *Curr. Opin. Microbiol.* **12**, 129–137 (2009).
2. M. Sola-Penna, D. Da Silva, W. S. Coelho, M. M. Marinho-Carvalho, P. Zancan, *IUBMB Life* **62**, 791–796 (2010).
3. C. Walsh, *Posttranslational Modification of Proteins: Expanding Nature's Inventory* (Roberts and Co., Englewood, CO, 2006).
4. T. Wang, R. Kartika, D. A. Spiegel, *J. Am. Chem. Soc.* **134**, 8958–8967 (2012).
5. S. G. Codreanu, B. Zhang, S. M. Sobecki, D. D. Billheimer, D. C. Liebler, *Mol. Cell. Proteomics* **8**, 670–680 (2009).
6. C. E. Paulsen *et al.*, *Nat. Chem. Biol.* **8**, 57–64 (2011).
7. A. Saiardi, R. Bhandari, A. C. Resnick, A. M. Snowman, S. H. Snyder, *Science* **306**, 2101–2105 (2004).
8. J. A. Demoss, S. M. Genuth, G. D. Novelli, *Proc. Natl. Acad. Sci. U.S.A.* **42**, 325–332 (1956).
9. S. H. Liaw, I. Kuo, D. Eisenberg, *Protein Sci.* **4**, 2358–2365 (1995).
10. M. P. Patricelli *et al.*, *Biochemistry* **46**, 350–358 (2007).
11. M. R. Larsen, T. E. Thingholm, O. N. Jensen, P. Roepstorff, T. J. Jørgensen, *Mol. Cell. Proteomics* **4**, 873–886 (2005).
12. E. L. Huttlin *et al.*, *Cell* **143**, 1174–1189 (2010).
13. Primary data (.RAW files) from mouse tissue phosphoproteomes (enriched by strong cation exchange chromatography and IMAC) as reported in (*12*), were downloaded from the Proteome Commons public database. MS2 files were generated with RAW Xtractor and searched for pgK modified peptides by using a mouse EBI-IPI forward-reverse proteomic database as discussed in Materials and Methods. False-positive rates were between 0.0 and 0.5%.
14. W. Huang, B. T. Sherman, R. A. Lempicki, *Nat. Protoc.* **4**, 44–57 (2009).
15. M. Mann, *Nat. Rev. Mol. Cell Biol.* **7**, 952–958 (2006).
16. B. J. Fueger *et al.*, *J. Nucl. Med.* **47**, 999–1006 (2006).
17. L. Zheng, R. G. Roeder, Y. Luo, *Cell* **114**, 255–266 (2003).
18. M. Kanwar, R. A. Kowluru, *Diabetes* **58**, 227–234 (2009).
19. E. C. Yego, S. Mohr, *J. Biol. Chem.* **285**, 3181–3190 (2010).
20. P. A. Sims, T. M. Larsen, R. R. Poyner, W. W. Cleland, G. H. Reed, *Biochemistry* **42**, 8298–8306 (2003).
21. A review of literature on glycolytic enzyme modification revealed evidence for phosphate-modified forms of GAPDH and ENO1 in bacteria, which were interpreted to potentially correspond to enzymes modified by adenosine diphosphate ribosylation and substrate (2-phosphoglycerate), respectively (*22*). Our data offer an additional interpretation of these findings as evidence that 1,3-BPG may also modify glycolytic enzymes in bacteria.
22. G. Boël *et al.*, *J. Mol. Biol.* **337**, 485–496 (2004).
23. P. A. Srere, *Annu. Rev. Biochem.* **56**, 89–124 (1987).
24. S. An, R. Kumar, E. D. Sheets, S. J. Benkovic, *Science* **320**, 103–106 (2008).
25. M. G. Vander Heiden, L. C. Cantley, C. B. Thompson, *Science* **324**, 1029–1033 (2009).
26. W. Yi *et al.*, *Science* **337**, 975–980 (2012).
27. R. Rosa, M. O. Prehu, Y. Beuzard, J. Rosa, *J. Clin. Invest.* **62**, 907–915 (1978).

Acknowledgments: We thank M. Dix and S. Niessen for assistance with mass spectrometry, C. Wang for support and advice on the use of CIMAGE software, and G. Simon for helpful discussions. Supported by the NIH (CA087660), the Damon Runyon Cancer Research Foundation (R.E.M. is a Howard Hughes Medical Institute Postdoctoral Fellow), and the Skaggs Institute for Chemical Biology.

Supplementary Materials

www.sciencemag.org/cgi/content/full/341/6145/549/DC1
Materials and Methods
Figs. S1 to S20
Tables S1 to S6
References (*28*–*39*)

26 March 2013; accepted 13 June 2013
10.1126/science.1238327